Early functional and transcriptomic changes in the myocardium predict outcome in a long-term rat model of sepsis

Rudiger, Alain ; Dyson, Alex ; Felsmann, Karen ; Carré, Jane E ; Taylor, Valerie ; Hughes, Sian ; Clatworthy, Innes ; Protti, Alessandro ; Pellerin, Denis ; Lemm, Jana ; Claus, Ralf A ; Bauer, Michael ; Singer, Mervyn

Abstract: Myocardial function is depressed in sepsis and is an important prognosticator in the human condition. Using echocardiography in a long-term fluid-resuscitated Wistar rat model of faecal peritonitis we investigated whether depressed myocardial function could be detected at an early stage of sepsis and, if so, whether the degree of depression could predict eventual outcome. At 6 h post-insult, a stroke volume <0.17 ml prognosticated 3-day mortality with positive and negative predictive values of 93 and 80%, respectively. Subsequent fluid loading studies demonstrated intrinsic myocardial depression with poor-prognosis animals tolerating less fluid than either good-prognosis or sham-operated animals. Cardiac gene expression analysis at 6 h detected 527 transcripts significantly up- or down-regulated by the septic process, including genes related to inflammatory and cell cycle pathways. Predicted mortality was associated with significant differences in transcripts of genes expressing proteins related to the TLR2/MyD88 (Toll-like receptor 2/myeloid differentiation factor 88) and JAK/STAT (Janus kinase/signal transducer and activator of transcription) inflammatory pathways, -adrenergic signalling and intracellular calcium cycling. Our findings highlight the presence of myocardial depression in early sepsis and its prognostic significance. Transcriptomic analysis in heart tissue identified changes in signalling pathways that correlated with clinical dysfunction. These pathways merit further study to both better understand and potentially modify the disease process.

DOI: https://doi.org/10.1042/CS20120334

Clinical Science (2013) **124**, 391–401 (Printed in Great Britain) doi: 10.1042/CS20120334

commentary online data

Original Paper

Early functional and transcriptomic changes in the myocardium predict outcome in a long-term rat model of sepsis

Alain RUDIGER*, Alex DYSON*, Karen FELSMANN†, Jane E. CARRÉ*, Valerie TAYLOR*, Sian HUGHES‡, Innes CLATWORTHY§, Alessandro PROTTI*, Denis PELLERIN‖, Jana LEMM¶, Ralf A. CLAUS¶, Michael BAUER¶[1] and Mervyn SINGER*

*Bloomsbury Institute of Intensive Care Medicine, Division of Medicine, University College London, Gower Street, London WC1E 6BT, U.K.
†SIRS-Lab GmbH, Otto-Schott-Strasse 15, D-07745 Jena, Germany
‡Department of Histopathology, Royal Free and University College Medical School, University College London, Rockefeller Building, University Street, London WC1E 6JJ, U.K.
§Imaging Facility, UCL Institute of Opthalmology, 11–43 Bath Street, London EC1V 9EL, U.K.
‖The Heart Hospital, UCL Hospitals NHS Foundation Trust, 16-18 Westmoreland Street, London W1G 8PH, U.K.
¶Integrated Research and Treatment Center–Center for Sepsis Control and Care, Jena University Hospital, Allee 101, D-07747 Jena, Germany

Abstract

Myocardial function is depressed in sepsis and is an important prognosticator in the human condition. Using echocardiography in a long-term fluid-resuscitated Wistar rat model of faecal peritonitis we investigated whether depressed myocardial function could be detected at an early stage of sepsis and, if so, whether the degree of depression could predict eventual outcome. At 6 h post-insult, a stroke volume <0.17 ml prognosticated 3-day mortality with positive and negative predictive values of 93 and 80%, respectively. Subsequent fluid loading studies demonstrated intrinsic myocardial depression with poor-prognosis animals tolerating less fluid than either good-prognosis or sham-operated animals. Cardiac gene expression analysis at 6 h detected 527 transcripts significantly up- or down-regulated by the septic process, including genes related to inflammatory and cell cycle pathways. Predicted mortality was associated with significant differences in transcripts of genes expressing proteins related to the TLR2/MyD88 (Toll-like receptor 2/myeloid differentiation factor 88) and JAK/STAT (Janus kinase/signal transducer and activator of transcription) inflammatory pathways, β-adrenergic signalling and intracellular calcium cycling. Our findings highlight the presence of myocardial depression in early sepsis and its prognostic significance. Transcriptomic analysis in heart tissue identified changes in signalling pathways that correlated with clinical dysfunction. These pathways merit further study to both better understand and potentially modify the disease process.

Key words: animal model, echocardiography, faecal peritonitis, gene transcript, heart failure, sepsis

INTRODUCTION

Sepsis, the systemic inflammatory response syndrome to infection, is the leading cause of death in the critically ill. This occurs primarily through the development of multiple organ failure [1], in which cardiac dysfunction is a well-recognized manifestation [2,3]. Identified mechanisms for myocardial depression include alterations in adrenergic signalling, intracellular calcium cycling, impaired electromechanical coupling and mitochondrial dysfunction [4]. The hierarchy of these mechanisms, however, remains uncertain and individual variations in severity inadequately explained.

A clinically relevant sepsis model achieving a 50% mortality rate raises the important but hitherto unaddressed question

Abbreviations: ARDB2 adrenergic receptor β_2; ATP2A3, ubiquitous calcium-transporting ATPase; CDKN1A, cyclin-dependent kinase inhibitor 1A; CI, confidence interval; COX2, cyclo-oxygenase 2; EM, electron microscopy; H&E, haematoxylin and eosin; HMBS, hydroxymethylbilane synthase; HR, heart rate; IL, interleukin; i.p., intraperitoneal; i.v., intravenous; JAK, Janus kinase; LBP, lipopolysaccharide-binding protein; LV, left ventricular; MyD88, myeloid differentiation factor 88; PDE10A, phosphodiesterase 10A; PKA, protein kinase A; PLA2G4A, phospholipase A_2 group IVA; PP1, protein phosphatase 1; PPP1CB, protein phosphatase 1 catalytic subunit β-isoform; PRKACA, protein kinase cAMP-dependent catalytic α; PRKAG2, protein kinase AMP-activated $\gamma 2$; PTGS2, prostaglandin-endoperoxidase synthase 2, ROC, receiver operator characteristic; SERCA, sarcoplasmic/endoplasmic reticulum Ca^{2+}-ATPase; SR, sarcoplasmic reticulum; STAT, signal transducer and activator of transcription; TLR, Toll-like receptor.

[1] A member of the scientific advisory board of SIRS-Lab GmbH, Jena, Germany, where the microarray experiments were performed.

Correspondence: Professor Mervyn Singer (email m.singer@ucl.ac.uk).

as to why some animals survive while the remainder die despite similar, if not, identical characteristics in terms of genotype, gender, age, weight and environment, and the septic insult received. Though these factors differ considerably in humans with sepsis, resulting in variable degrees and combinations of multiple organ dysfunction, a wide selection of inflammatory [5], hormonal [6,7], circulatory [8], bioenergetic [9] and organ dysfunction biomarkers [7,10] can prognosticate as early as the first few days of intensive care admission. Notably, survivors and non-survivors are often clinically indistinguishable at this early time point. This implies that mortality may be determined to a large extent by a pattern of molecular genetic and functional responses that differentiate survivors from non-survivors at an early stage.

Although the degree of myocardial depression has been reported in several clinical studies to be an indicator of poor outcome [11,12], others suggest this may have a protective role [13]. This disparity may relate to timing of the study relative to the duration of critical illness. However, the role and prognostic significance of early myocardial dysfunction has received relatively scant attention. We hypothesized that early cardiac performance could predict eventual outcome, and performed transcriptomic analysis to probe putative pathways that could reconcile the physiological and molecular mechanisms of sepsis-induced cardiac dysfunction.

MATERIALS AND METHODS

Animal model

All experiments were performed according to local ethics committee (University College London) and Home Office (U.K.) guidelines under the 1986 Scientific Procedures Act. Under 2% isoflurane anaesthesia, male Wistar rats (Charles River) had PVC tubes (inner diameter, 0.58 mm; outer diameter, 0.96 mm) inserted into the right jugular vein and left carotid artery, and tunnelled subcutaneously to emerge at the nape of the neck. These lines were subsequently mounted on to a swivel-tether system allowing the rat, on recovery from anaesthesia, to have unimpeded movement in its cage and free access to food and water. After 24 h, sepsis was induced by i.p. (intraperitoneal) injection of faecal slurry (1.8 ml of a 40% preparation obtained from the bowel content of a rat from the same batch). Fluid resuscitation, consisting of a 1:1 solution of 6% hetastarch (Elohaes®; Fresenius-Kabi) and 5% glucose, was commenced 2 h later through the central venous line. Glucose supplementation prevented hypoglycaemia in the animals with sepsis due to decreased appetite and intake. The infusion rate was maintained at 10 ml/kg of body weight per h between 2 h and 24 h, halving thereafter at 24 h intervals. Animals received additional 25 ml/kg of body weight boluses of 6% hetastarch at 6 h and 10 ml/kg of body weight at 24 h to optimize fluid resuscitation (results from pilot studies). Sham animals of similar age, gender and weight underwent identical instrumentation and fluid administration, but did not receive the i.p. injection of faecal slurry. At 6, 24, 48 and 72 h post-sepsis induction, and in sham-operated controls, clinical scoring was performed. This included an assessment of appearance, alertness and movement, as previously described [14].

Echocardiography

Echocardiography studies were carried out using a 14 MHz linear-array transducer connected to a digital ultrasound system (Vivid 7; GE Healthcare). Images were acquired in left parasternal long and short axis views at the papillary muscle level. Radius (r) and length (l) of the left ventricle were measured at end-diastole by M-mode and two-dimensional mode respectively. LV (left ventricular) end-diastolic volumes were calculated using a prolate spheroid formula ($4/3 \cdot \pi \cdot r^2 \cdot l$). Stroke volume was measured in the ascending aorta (radius 1.3 mm) from the velocity–time integral using pulsed-wave Doppler. The vessel diameter at this level remains stable despite intravascular volume variations [15].

Study 1: long-term outcome study

A total of 20 rats with sepsis and eight sham-operated rats (body weight, 334 ± 4.5 g) were monitored for 72 h, and time of death was recorded. At baseline, 3, 6, 24, 48 and 72 h, spontaneously breathing animals were removed from their cage, anaesthetized with isoflurane and placed in a supine position on a warming mat for echocardiography. The concentration of isoflurane was kept between 1.0 and 1.5%, so that the animals tolerated the study but could react to a leg pinch with a withdrawal response.

Study 2: fluid loading study

In 14 rats with sepsis and six sham rats (body weight, 305 ± 6.0 g) i.v. (intravenous) fluid resuscitation was started 2 h after the insult with echocardiography performed at 6 h, as described above. Following echocardiography, animals received a 2.5 ml bolus (approximately 8 ml/kg of body weight) of 6% hetastarch intravenously over 2 min, and this was repeated at approximately 5 min intervals. Echocardiography was performed immediately after each fluid bolus. Bolus fluid administration was repeated until death occurred.

Study 3: histology

Two sham animals and 11 animals with sepsis were prepared as above. At 6 h post-insult, echocardiography was performed to distinguish predicted sepsis survivors from non-survivors. Animals were killed at 24 h. Cardiac samples for histology and EM (electron microscopy) were taken from the LV free wall at the papillary muscle level and were analysed by blinded investigators.

Study 4: network-based gene expression analysis

The model was prepared as described above. At 6 h post-insult, clinical severity was recorded [14] and echocardiography performed to distinguish predicted survivors from non-survivors. Freshly culled (naïve) and sham-operated animals served as controls. Hearts (four per group) were promptly removed and stored in liquid nitrogen. Heart muscle samples (30–50 mg each) were transferred into 900 μl of lysis solution (RNeasy Mini Kit; Qiagen) including mercaptoethanol, homogenized in a tissue lyser at 30 Hz for 4 min at room temperature (Qiagen), then

Table 1 Differences at 6 h between sham animals, sepsis survivors and sepsis non-survivors

Parameters were recorded at 6 h, before administration of the fluid bolus. Values represent means (±S.E.M.). Ejection fraction (EF) was calculated as (stroke volume/end-diastolic volume)×100. *$P < 0.05$ compared with sepsis survivors; †$P < 0.05$ compared with sepsis non-survivors; ‡$P < 0.05$ compared with sham controls. LV, EDV, LV end-diastolic volume; IVC, inferior vena cava; MAP, mean arterial pressure.

Parameter	Sham ($n = 8$)	Sepsis survivors ($n = 5$)	Sepsis non-survivors ($n = 15$)
Core temperature (°C)	36.9 (±0.21)	37.2 (±0.36)	38.0 (±0.32)
Respiratory rate (breaths/min)	76 (±2.8)	78 (±5.9)	86 (±3.4)
MAP (mmHg)	129 (±9.2)	127 (±5.0)	133 (±4.1)
HR (beats/min)	411 (±14)	404 (±20)†	491 (±10)‡
LV EDV (ml)	0.52 (±0.02)*	0.37 (±0.02)	0.30 (±0.02)‡
Stroke volume (ml)	0.27 (±0.02)	0.21 (±0.03)†	0.12 (±0.01)‡
Cardiac output (ml/min)	111 (±3.5)	86 (±14)	60 (±4.7)‡
LV EF (%)	53 (±2.4)	55 (±7.0)	43 (±3.5)
IVC diameter (mm)	0.30 (±0.02)	0.24 (±0.03)	0.20 (±0.01)‡

centrifuged and processed further, according to manufacturer's instructions. RNA integrity and purity were analysed (Agilent 2100; Agilent), and 300 ng of total RNA was reverse-transcribed and amplified (Illumina RNA amplification Kit IL1791; Ambion). All cRNA samples were quantified with a NanoDrop spectrophotometer before proceeding to sample hybridization. A portion (0.75μg of cRNA) of each sample was hybridized to Sentrix Rat Ref-Seq-12 Beadchips (BD-27-302; Illumina) with >24 000 gene-specific oligonucleotide probes per array, targeting all known genes and splice variants. The hybridized arrays were stained with Streptavidin-Cy3 (FluoroLinkTM Cy3^{TM}; Amersham Biosciences), diluted to 1 mg/ml or 1 μg/μl with RNase-free water, washed, dried and scanned immediately on the Illumina Bead Station. Data were normalized using a variance stabilizing transformation [16]. For the heatmap, the expression values of selected genes were Z-score standardized (S.D. = 1, mean = 0). Data were analysed using Ingenuity Pathway Analysis (Ingenuity Systems) for functional analyses of the dataset to identify significant biological functions and diseases connected with the expression profile. The microarray experiment description file according to the MIAME checklist is available at ftp://rudiger2012:Phee5eTh@ftp.sirslab.de/

To confirm changes in mRNA transcript levels, ATP2A3 (ubiquitous calcium transporting ATPase), PRKAG2 (protein kinase AMP-activated protein kinase γ2 non-catalytic subunit), PRKACA (protein kinase cAMP-dependent catalytic α) and PPP1CB (protein phosphatase 1 catalytic subunit β-isoform) were quantified by real-time PCR. Results were computed with specialized software (qBase plus; Biogazelle) and given as the ratio between the gene of interest and the housekeeping gene HMBS (hydroxymethylbilane synthase).

Statistics

Results are expressed as means ± S.E.M. or percentages. Continuous variables were compared with ANOVA. If appropriate, post-hoc testing was performed using Bonferroni corrections. χ^2 testing compared the categorical variables. The quality of stroke volume as a diagnostic test was described by the area under the ROC (receiver operator characteristic) curve. Relationships between gene array and PCR values are described by the square of the sample correlation coefficient. All testing was two-tailed; P values <0.05 were considered significant.

RESULTS

Study 1: long-term outcome study

Animals with sepsis developed clinical manifestations of illness including hunched appearance, piloerection, bloating and lethargy, reaching a nadir between 16–48 h. A spectrum of clinical severity was observed, even between animals from the same litter, which received the same batch of faecal slurry. Animals with sepsis showed early signs of sepsis at 6 h after i.p. slurry injection; their clinical severity score of 2.6 ± 0.4 contrasted with 0 ± 0 for sham animals ($P < 0.001$). However, the clinical severity was similar between animals predicted to survive or not. Survival rates at 6, 24, 48 and 72 h were 95, 55, 30 and 25% respectively. At post-mortem, purulent peritonitis was present with ascites, adhesions and enlarged, fluid-filled bowel loops. Survivors showed signs of recovery by 72 h with increased interest in their surroundings, improved appetite and appearance. Sham animals became oedematous yet continued to eat, drink and maintain an interest in their environment. One sham animal developed a local wound infection at the tether anchorage site. Two other sham animals developed right ventricular dilatation, with one dying between 48 and 72 h. All available results are included in the analyses. Clinical and haemodynamic parameters are displayed in Table 1 and Figure 1. Fluid resuscitation, starting at 2 h and optimized by a fluid bolus at 6 h, restored preload deficiency in the animals with sepsis. As a result of the fluid loading, stroke volume and, consequently, cardiac output increased in all groups.

Stroke volume measured at 6 h was a good discriminator of outcome, with an area under the ROC curve of 0.83 [95% CI (confidence interval), 0.57–1.1; $P =$ 0.033]. A total of 13 out of the 14 animals with a stroke volume <0.17 ml died (mortality 93%) compared with one of five animals with a stroke volume ⩾0.17 ml (mortality 20%, $P =$ 0.006). Hence a 6 h stroke volume <0.17 ml could prognosticate 3-day mortality with high positive and negative predictive

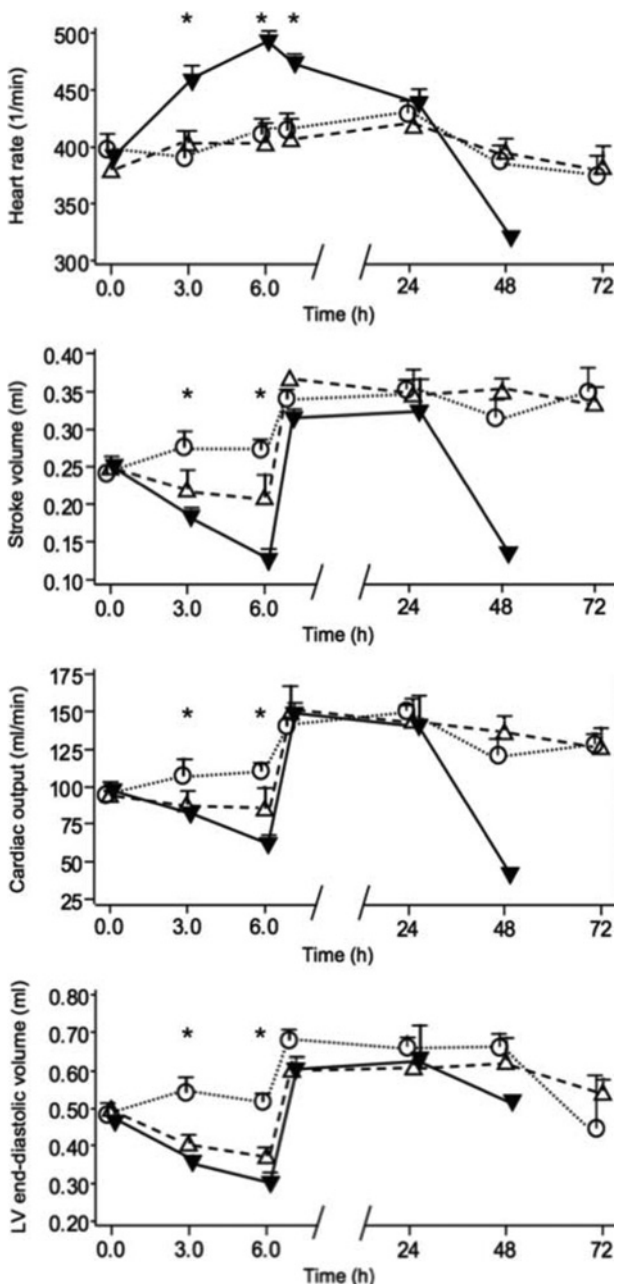

Figure 1 Temporal changes in haemodynamics

○, Sham animals ($n = 8$); △, sepsis survivors ($n = 5$); ▼, sepsis non-survivors ($n = 15$). Values represent means ± S.E.M. Fluid resuscitation was commenced 2 h after sepsis induction. The infusion rate was maintained at 10 ml/kg of body weight per between 2 h and 24 h, and halving thereafter at 24 h intervals. Animals received additional 25 ml/kg of body weight fluid boluses at 6 h and 10 ml/kg of body weight at 24 h to optimize fluid resuscitation. One sham animal died between 48 and 72 h. Significant differences between groups ($P < 0.05$ by ANOVA) were found for all four variables at 3 and 6 h (prior to fluid loading). After the fluid bolus at 6 h, the group difference was only significant for HR.

values of 93 and 80%, respectively. Consequently, this cut-off value was used in subsequent experiments to distinguish predicted survivors from non-survivors. Unlike body temperature and clinical severity, HR (heart rate) measured at 6 h could also discriminate outcomes [ROC 0.93 (95% CI, 0.81–1.0); $P = 0.005$], with similar positive (93%) and negative (80%) predictive values. Animals with sepsis with a HR ⩾430/min had a mortality of 93%, whereas those with a HR below this cut-off had a 3-day mortality of only 20% ($P = 0.006$). Supplementary Table S1 (at http://www.clinsci.org/cs/124/cs1240391add.htm) shows the reproducibility of the echocardiography parameters.

Study 2: fluid loading study

Figure 2(A) shows changes in stroke volume with repeated fluid administration. Predicted non-survivors were fluid-responsive but failed to reach maximal stroke volumes attained by predicted survivors or sham-operated animals. Total volume infused before death was 31 ± 7.3 ml in predicted non-survivors, 49 ± 6.4 ml in predicted survivors and 61 ± 5.6 ml in sham animals ($P < 0.05$). Right ventricular dilatation with increasing septal shift and impaired LV filling, suggestive of right heart failure, was seen as a pre-terminal event (Figure 2B).

Study 3: histology

Only three out of 11 animals with severe sepsis survived until 24 h in this substudy. Tissues from these three animals were compared with tissues from two sham controls. H&E (haematoxylin and eosin)-stained cardiac tissues showed no signs of necrosis and minimal immune cell infiltration. Oil Red-O staining failed to demonstrate intracellular lipid accumulation. EM of hearts from animals with sepsis revealed glycogen accumulations along clusters of mitochondria and between myofibrils. Although the contractile apparatus appeared normal, many mitochondria showed morphological derangements (Figure 3).

Study 4: network-based gene expression analysis

Gene expression profiling of heart tissue from naïve, sham, and predicted sepsis survivor and sepsis non-survivor subgroups revealed 527 significantly altered gene transcript activities. Figure 4 shows the differences in mean gene expression values between the groups, displayed as four clusters of co-regulated transcripts. Cluster 2 represents transcripts of decreased abundance related to anaesthesia and instrumentation. These differed significantly in amount between naïve and sham rats; sepsis did not further alter these transcript levels so this can be interpreted as an 'injury' cluster. Here, Ingenuity Pathway Analysis revealed a pronounced effect on transcript levels reflecting tissue proliferation status (cell cycle and replication), and a decrease in cAMP signalling transcripts. Cardiac actin and mitochondrial ribosomal protein transcripts were also decreased. In addition, down-regulation of ARDB2 (adrenergic receptor β_2) and PRKCA (protein kinase Cα) may have contributed to the cardiac dysfunction observed in the animals with sepsis by providing an initial basic trigger for subsequent sepsis-specific signalling in the adrenergic pathway. Cluster 4 represents transcripts elevated in sham-operated compared with naïve animals, but not further affected by sepsis. Hence, this can be interpreted as a 'danger' cluster.

Clusters 1 and 3 represent the changes in transcripts specific to sepsis. Supplementary Table S2 (at http://www.clinsci.org/cs/124/cs1240391add.htm) lists all of the increased (65 genes) and decreased (55 genes) transcripts in predicted

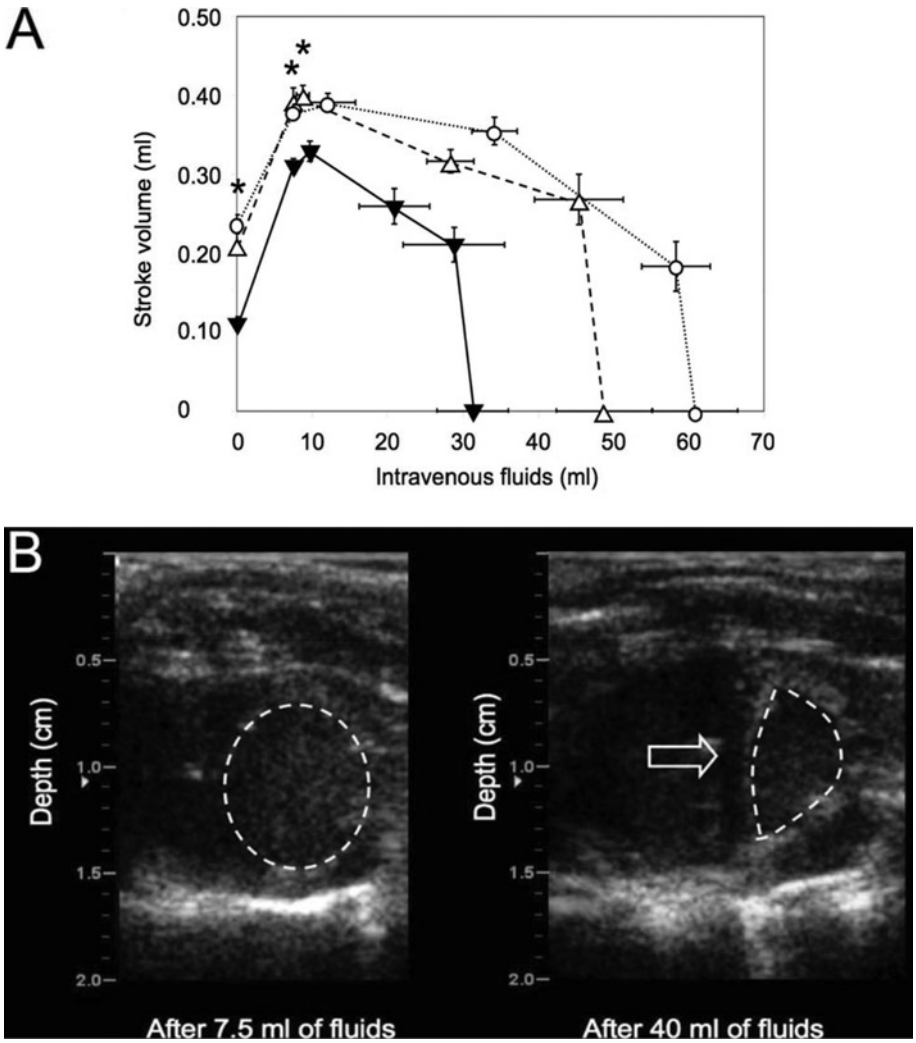

Figure 2 **Fluid loading study**

(**A**) Animals with sepsis were classified into predicted non-survivors (▼) [defined by 6 h stroke volume <0.17 ml ($n = 8$)], and predicted survivors (Δ) [defined by stroke volume ⩾0.17 ml ($n = 6$)]. Sham animals (○) served as controls ($n = 6$). Values shown illustrate mean stroke volumes at baseline (6 h post-sepsis induction) and post-administration of hetastarch (25 ml/kg of body weight), maximal stroke volumes reached, intermediate values, pre-terminal values and at death (= stroke volume 0 ml). Error bars represent S.E.M. Significant differences ($P < 0.05$ by ANOVA) in stroke volume were seen between groups at baseline, after 7.5 ml of fluid, and at maximal stroke volume attained. (**B**) Two-dimensional echocardiography images acquired in a rat with sepsis at 6 h using parasternal short-axis view at end-diastole. Left-hand panel: post-administration of 7.5 ml of hetastarch, the left ventricle (broken line) is not compromised, whereas the right ventricle is hardly visible. Right-hand panel, after administration of 40 ml of hetastarch, the right ventricle is dilated, the septum (arrow) is flattened and compromises LV filling (broken line).

non-survivors compared with survivors. To study sepsis-specific events in more detail, subsequent analyses focused on these two clusters. Compared with the sham group, the main signalling pathways affected by sepsis were the acute-phase response plus TLR (Toll-like receptor), IL (interleukin)-6 and IL-10 signalling. As depicted for the TLR and IL-6 signalling pathways (Figure 4C), central players of innate immunity [e.g. TLR2, MyD88 (myeloid differentiation factor 88), LBP (lipopolysaccharide-binding protein) and the JAK/STAT (Janus kinase/signal transducer and activator of transcription) pathway] responded with an increase in transcript abundance. Ingenuity Pathway Analysis of the sepsis-regulated transcripts revealed profound effects on gene expression activities in animals with sepsis, including the functional categories of inflammatory disease, organ injury and abnormalities, skeletal and muscular disorders, and cardiovascular disease. Transcript levels of STAT3, REL, c-Myc, BCL10 and p21, potent regulators of proliferation and apoptosis at the transcription level, were increased in response to sepsis. Key mediators of inflammation such as PLA2G4A (phospholipase A_2 group IVA), PTGER4 (prostaglandin E receptor 4) and PTGS2 [prostaglandin-endoperoxidase synthase 2: COX2 (cyclo-oxygenase 2)] were likewise elevated.

Pathways associated with predicted poor outcome included transcripts encoding for amino-sugar metabolism [PDE10A

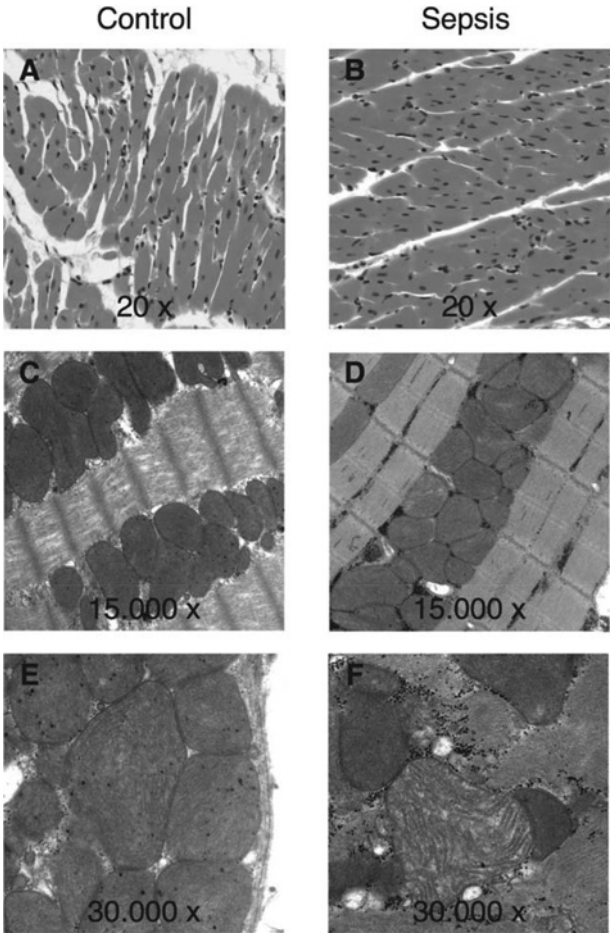

Figure 3 Histological analysis
Light and EM of cardiac tissue in different magnifications taken from a sham animal (left-hand panels), and 24 h post-sepsis induction from a predicted non-survivor (right-hand panels). (**A** and **B**) Using light microscopy (H&E staining), normal cardiac structures with minimal immune cell infiltration are shown. (**C** and **D**) Structural integrity of the myofibrillar apparatus using EM. (**E**) Normal mitochondria at higher magnification in a sham animal. (**F**) A mitochondrion with adjacent glycogen accumulations in a heart taken from an animal with sepsis. The swollen less electron-dense appearance of the mitochondrion suggests organelle damage.

(phosphodiesterase 10A), UAP1 (UDP-N-acetylglucosamine pyrophosphorylase 1) and CYB5R2 (cytochrome b_5 reductase 2)] and p53-dependent cell-cycle arrest [CDKN1A (cyclin-dependent kinase inhibitor 1A), GADD45G (growth-arrest and DNA-damage-inducible protein 45G) and STAG1 (stromal antigen 1)]. Consistent with the progressive worsening in myocardial function demonstrated physiologically, significant differences in transcripts within the β-adrenergic signalling and calcium-cycling pathways were also linked with an unfavourable outcome (Figure 5). These included increases in PDE10A, PP1 (protein phosphatase 1) and ITPKC (inositol 1,4,5-trisphosphate 3-kinase C) and decreased SERCA (sarcoplasmic/endoplasmic reticulum Ca^{2+}-ATPase). In addition, the PKA (protein kinase A) transcript was decreased in animals with sepsis compared with sham animals. The correlations between gene array and PCR results were good for ATP2A3 and PRKAG2, moderate for PRKACA and absent for PPP1CB (see Supplementary Figure S1 and Supplementary Table S3 at http://www.clinsci.org/cs/124/cs1240391add.htm).

DISCUSSION

In the present study, we describe a clinically relevant fluid-resuscitated long-term (3-day) rodent model of sepsis where outcome could be determined with high accuracy from haemodynamic measurements taken early in the illness. This demonstration of an early difference in phenotype in animals that proceeded to either recover fully or die occurred notwithstanding similarities in genotype, age, gender and upbringing of these animals, and receipt of a similar insult. They reflect patient data where, despite the marked heterogeneity of patient populations, baseline cardiovascular variables such as HR [8,17], stroke volume [18] and cardiac output [18,19] could differentiate between survivors and non-survivors of septic shock. We used echocardiography-derived measurements of stroke volume for the present study, which predicted mortality with a high positive and negative predictive value. Though our focus was on ventricular performance, we also found a similar predictive ability could be made for HR. This may offer a viable option for future studies if the capability to measure stroke volume is not available. Our findings suggest that an increased systemic inflammatory response will compromise myocardial function through circulating myocardial depressant factors [20] including NO (nitric oxide) [21], and through altered gene expression of proteins involved in cardiac contractile and relaxation pathways (as demonstrated at 6 h in the present study) and, subsequently (at 12–48 h), in bioenergetic pathways [22].

The lower values of cardiac output in the predicted non-survivor group did not simply reflect more profound hypovolaemia related to a greater degree of capillary leak, as fluid loading failed to generate either the maximal stroke volumes attained by the sham or sepsis survivor groups, nor did it reduce HR. Notably, all animals with sepsis at 6 h were normotensive (Table 1) and had received 40 ml/kg of body weight (equivalent to 3 litres in humans) between 2 and 6 h. Intrinsic myocardial depression was, however, confirmed by a progressive decrease in tolerance to large volume fluid loading in the animals with sepsis; this occurred to a much greater extent in predicted non-survivors.

Hollenberg et al. [23] reported myocardial depression in mice with sepsis, despite the co-existence of a high cardiac output. These findings reflect those made in clinical echocardiographic studies, some of which could also prognosticate as early as the first day of ICU (intensive care unit) admission [12,24,25]. As seen in this study, the failing thinner-walled right ventricle copes less well with excessive fluid loading; this will likely be compounded in sepsis by co-existing (acute) lung injury, increasing pulmonary artery pressures and right ventricular afterload. A careful balance must therefore be reached between an avoidance of excess fluid that will compromise myocardial function and worsen interstitial oedema [26], and sufficient fluid administration to rescue the macrocirculation, improve organ perfusion and enhance survival [26]. As our data demonstrate, the sicker the animals with sepsis become, the less fluid loading they are able to tolerate.

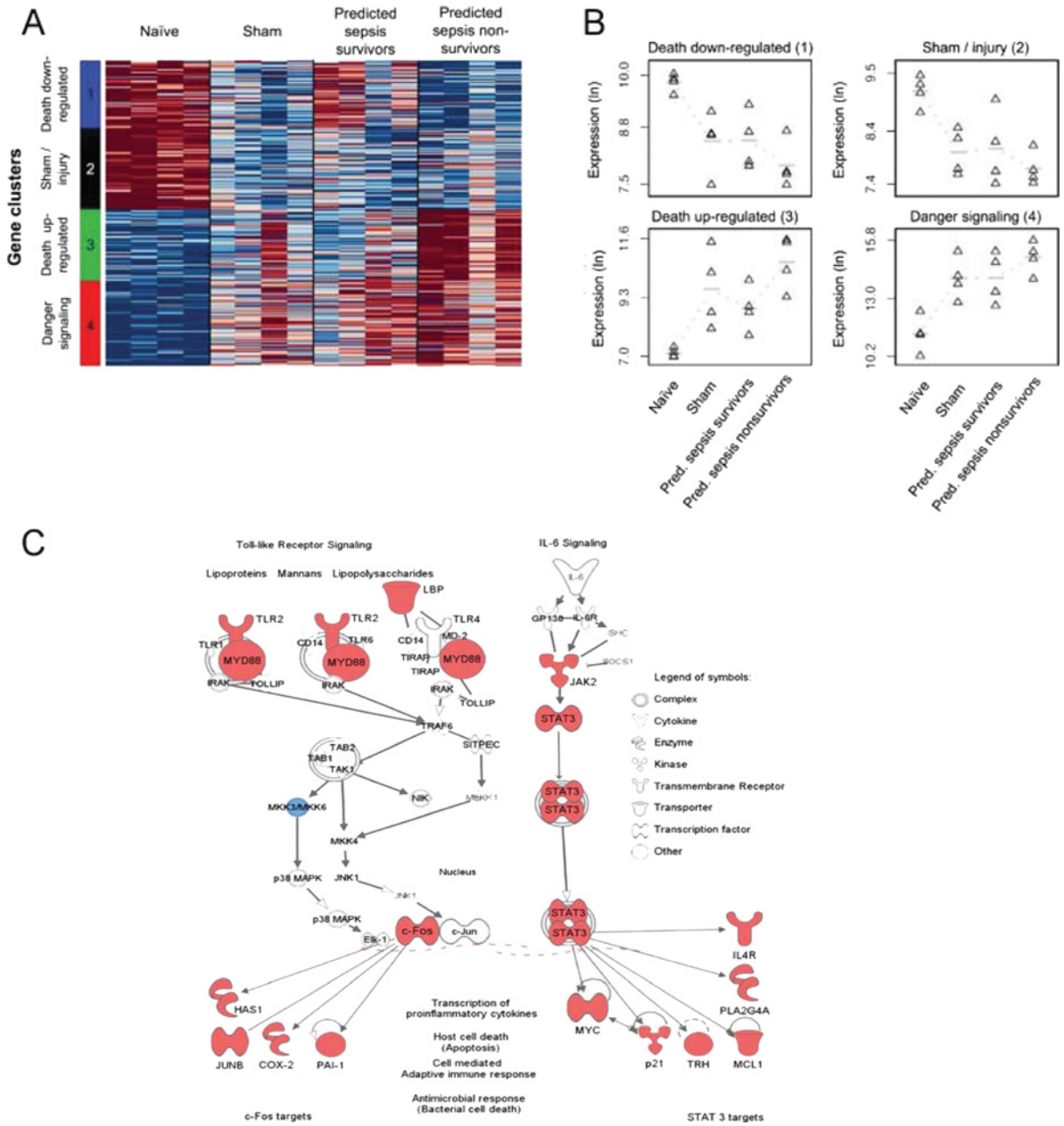

Figure 4 **Network-based gene expression analysis**

(**A**) Heatmap highlighting significant differences in 527 mean gene expression values between the four clinical groups ($n = 4$ per group). These are displayed as four clusters of transcripts with similar gene activity patterns. Associated colours represent variance-normalized expression values relative to the mean expression of each transcript within this experiment. Red and blue indicate relative increase or decrease of transcript abundance, respectively. (**B**) Gene expression values of one representative transcript for each of the four clusters, illustrating the relative transcript abundance in each cluster. For cluster 1: Cited4 [CBP (cAMP-response-element-binding protein) interacting transactivator-4], cluster 2: Nrep (neuronal protein 3.1), cluster 3: SELP (selectin-P) and cluster-4: Mt1a (metallothionein-1a). (**C**) Signalling pathways most prominently activated/altered in the sepsis cluster (cluster 3). Both TLR and IL-6 signalling lead to transcriptional activation of central regulators of proliferation, cell death and immune response. MKK3/MKK6, mitogen-activated-protein-kinase kinase 3/6, PAI-1, plasminogen activator inhibitor-1, HAS-1, hyaluronan synthase-1; TRH, thyrotropin-releasing hormone, MCL, myeloid cell leukaemia sequence 1 (BCL2-related), IL4R: IL-4 receptor. The Ingenuity Pathway Analysis Figure is

Histology demonstrated negligible cardiac tissue necrosis, supporting previous findings in animals with sepsis [15,27,28] and in non-survivors of human septic shock [29,30]. EM did display evidence of mitochondrial swelling, suggesting organelle damage, confirming previous work by ourselves and others in animals [21,22,28,31–33] and patients [34] with sepsis. The finding of glycogen accumulation in cardiomyocytes from animals with sepsis, as reported previously [35], has also been identified in

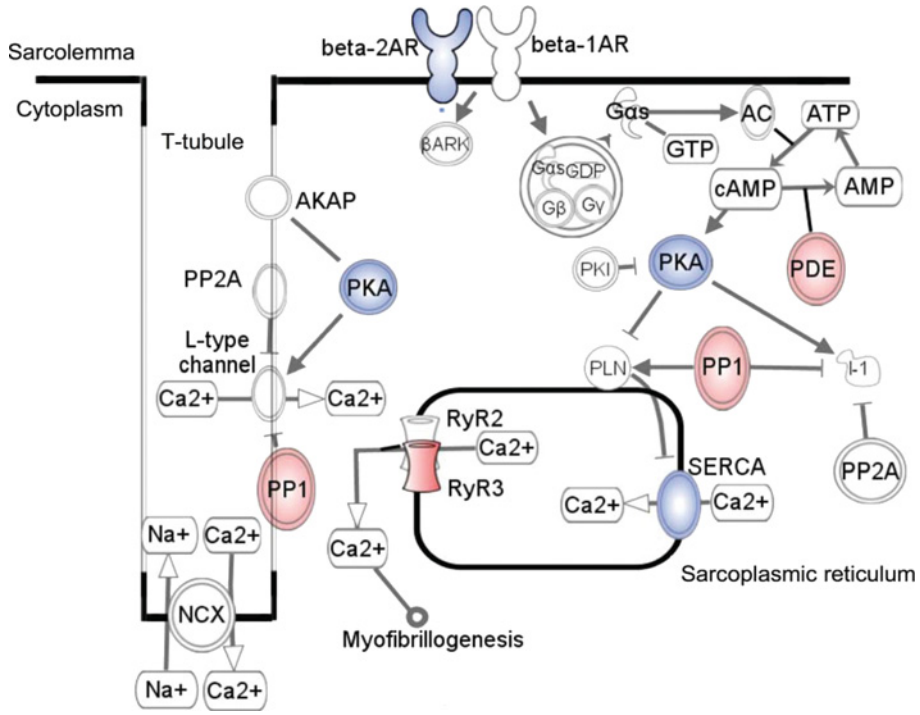

Figure 5 Myocardial transcriptomics revealing transcript alterations in β-adrenergic signalling and Ca^{2+} flux pathways depending on disease severity

Cardiomyocyte contraction depends on intracellular Ca^{2+} regulated by catecholamines acting on the ARβ_2, with subsequent activation of G_s (stimulatory G-proteins) and elevation of cAMP. This activates PKA, phosphorylating PLN (phospholamban), an SR transmembrane protein. Depending on its own phosphorylation state, PLN promotes the active state of the Ca^{2+} ATPase SERCA, favouring Ca^{2+} uptake into the SR. PP1 dephosphorylates PLN, deactivating SERCA. Ca^{2+} entry into the cell through L-type calcium channels triggers Ca^{2+}-mediated Ca^{2+} release from the SR via RyRs (ryanodine receptors). This dictates the degree of actin–myosin cross-bridge formation and the strength of contraction. Relaxation occurs when cytosolic Ca^{2+} is lowered primarily by activity of SERCA, as well as plasmalemmal Ca^{2+}-ATPases and Na^+/Ca^{2+} exchangers. Compared with predicted survivors, predicted non-survivors showed increased (red) cardiac gene transcripts for PDE10 (phosphodiesterase 10), PP1 and RyR3, whereas SERCA transcript abundance was decreased (blue). The β_2AR (β_2-adrenergic receptor) and PKA transcript levels were decreased in hearts from animals with sepsis, but did not reach statistical significance between predicted survivors and non-survivors. The Ingenuity Pathway Analysis Figure is

hibernating myocardium of pigs following ischaemia [36]. In summary, structural tissue damage was minor, although changes were apparent at the subcellular level. These observations support our hypothesis that myocardial dysfunction is a functional rather than a structural derangement [4,37].

This descriptive approach to myocardial depression in sepsis can be systematically studied in the present model by applying genome-wide analysis of alterations in the myocardial transcriptome. To this end, we employed a structured network knowledge-based approach that can provide insights into regulation of cell function and interaction, as demonstrated in healthy volunteers treated with endotoxin [38]. Although we cannot yet describe precise mechanisms through which these changes occur, sepsis clearly elicits significantly different responses compared with sham operation alone, and that some of these are differentially expressed and associated with poor outcome.

The genome-wide profiling revealed early up-regulation of TLR2/MyD88 and JAK/STAT3-dependent signalling with sepsis. This supports findings of improved cardiac function, with normal sarcomere shortening and peak change in intracellular Ca^{2+}, in TLR2$^{-/-}$ mice undergoing caecal ligation and puncture compared with their wild-type equivalents [39]. Although the JAK/STAT3 pathway is generally considered to be cardioprotective [40], it too can contribute to cardiac dysfunction during ischaemia [41]. A study of rats undergoing cecal ligation and puncture reported attenuated organ failure and improved survival rates following JAK/STAT3 pathway inhibition, although the heart was not specifically examined [42].

Importantly, in relation to the physiological changes recorded in this model, myocardial transcriptomics revealed alterations in transcript abundance linked to β-adrenergic signalling and Ca^{2+} flux that depended on disease severity and prognosis (Figure 5). Although mindful of the limitations in interpreting transcriptomic data, it is conceivable that such transcript differences could impact on myocardial function. In our model, the PKA transcript level was significantly decreased in the animals with sepsis, whereas PDE10 transcript abundance was elevated. PDE increases breakdown of cAMP, further reducing PKA activity [43]. Increased activity of PP1 dephosphorylates phospholamban, reducing Ca^{2+} uptake into the SR (sarcoplasmic reticulum) [44]. Down-regulation of SERCA has a similar effect [45]. Up-regulation of PP1 and down-regulation of PKA also reduce Ca^{2+}

entry into the cell by inhibiting L-type calcium channels [46]. A diminution in L-type calcium current was reported recently in ventricular myocytes isolated from pigs with sepsis [47]. High cytosolic and low SR Ca^{2+} levels lead to failure of diastolic relaxation and impaired systolic contraction, respectively. Both these aspects are also recognized in septic cardiomyopathy [4,48].

We focused our transcriptomic analyses on heart tissue as our prognostic tool was based on an assessment of myocardial dysfunction. Analyses of liver tissue taken concurrently show significant differences in other signalling pathways [49]. It is thus reasonable to speculate that each organ has its own transcriptomic response to infection. A better understanding of each organ's response, and interactions between organs, may provide useful clues to developing novel therapies.

In summary, our findings emphasize both the presence and prognostic significance of cardiac dysfunction with intrinsic myocardial depression during early sepsis, at a time when overall clinical severity was not marked. The poor-prognosis animals had reduced tolerance to i.v. fluid loading, highlighting the importance of adequate but not excessive fluid administration in clinical management. Our study implies that outcome is already determined at an early stage in sepsis. Greater or lesser degrees of gene up- or down-regulation, with the likely addition of post-transcriptional modifications that were not measured in this study, will distinguish eventual survivors and non-survivors. If confirmed, this has major consequences for patient management as a proportion are clearly not benefiting from current approaches; new paradigms would need to be introduced to improve outcomes in such patients.

CLINICAL PERSPECTIVES

- Myocardial function is depressed in sepsis and is an important prognosticator in patients.
- Using a long-term fluid-resuscitated rat model of faecal peritonitis, we demonstrate that significant differences in stroke volume and HR measured 6 h post-insult could predict 3-day mortality with positive and negative predictive values of 93 and 80% respectively. In separate studies, cardiac gene expression analysis at 6 h detected 527 transcripts significantly up- or down-regulated by the septic process, including genes related to inflammatory and cell cycle pathways. The degree of change in these signalling pathways correlated with clinical dysfunction.
- These findings suggest a crucial role for early cardiovascular performance in determining subsequent outcome, with clear therapeutic implications.

AUTHOR CONTRIBUTION

Alain Rudiger conceived and designed the study, performed the experimental work, analysed and interpreted the data, and drafted and approved the paper. Alex Dyson, Karen Felsmann and Jane Carré performed the experimental work, and drafted and approved the paper. Valerie Taylor performed the experimental work. Sian Hughes performed the experimental work and interpreted the data. Innes Clatworthy, Jana Lemm and Ralf Claus performed the experimental work and interpreted the data. Alessandro Protti and Denis Pellerin assisted with experimental design and interpreted the data. Michael Bauer interpreted the data, and drafted and approved the paper. Mervyn Singer conceived and designed the study, interpreted the data, supervised the study, and drafted and approved the paper.

FUNDING

This work was supported by the Swiss National Science Foundation (Basel, Switzerland), the Stiefel Zangger Foundation (Zurich, Switzerland) and the Siegenthaler Foundation (Zurich, Switzerland) (grants to A.R.), and the U.K. Medical Research Council (grants to A.D., J.C. and V.T.). The echocardiography equipment was funded by the British Heart Foundation. Transcriptomic analyses were funded by the Krokus Foundation (Basel, Switzerland) (to A.R.), and the Federal Ministry for Education and Research (within the 'Center for Sepsis Control and Care') [grant number 01 EO 1002, Project D1.2 (to M.B.)]. This work was undertaken at UCL Hospitals/UCL, which received support from the National Institute of Health Research Biomedical Research Centre funding scheme.

REFERENCES

1 Hotchkiss, R. S. and Karl, I. E. (2003) The pathophysiology and treatment of sepsis. N. Engl. J. Med. **348**, 138–150
2 Levy, R. J. and Deutschman, C. S. (2004) Evaluating myocardial depression in sepsis. Shock **22**, 1–10
3 Vieillard-Baron, A., Caille, V., Charron, C., Belliard, G., Page, B. and Jardin, F. (2008) Actual incidence of global left ventricular hypokinesia in adult septic shock. Crit. Care Med. **36**, 1701–1706
4 Rudiger, A. and Singer, M. (2007) Mechanisms of sepsis-induced cardiac dysfunction. Crit. Care Med. **35**, 1599–1608
5 Hein, O. V., Misterek, K., Tessmann, J. P., van Dossow, V., Krimphove, M. and Spies, C. (2005) Time course of endothelial damage in septic shock: prediction of outcome. Crit. Care **9**, R323–R330
6 Angstwurm, M. W., Gaertner, R. and Schopohl, J. (2005) Outcome in elderly patients with severe infection is influenced by sex hormones but not gender. Crit. Care Med. **33**, 2786–2793
7 Brueckmann, M., Huhle, G., Lang, S., Haase, K. K., Bertsch, T., Weiss, C., Kaden, J. J., Putensen, C., Borggrefe, M. and Hoffmann, U. (2005) Prognostic value of plasma N-terminal pro-brain natriuretic peptide in patients with severe sepsis. Circulation **112**, 527–534
8 Parker, M. M., Shelhamer, J. H., Natanson, C., Alling, D. W. and Parrillo, J. E. (1987) Serial cardiovascular variables in survivors and nonsurvivors of human septic shock: heart rate as an early predictor of prognosis. Crit. Care Med. **15**, 923–929
9 Brealey, D., Brand, M., Hargreaves, I., Heales, S., Land, J., Smolenski, R., Davies, N. A., Cooper, C. E. and Singer, M. (2002) Association between mitochondrial dysfunction and severity and outcome of septic shock. Lancet **360**, 219–223
10 Ammann, P., Maggiorini, M., Bertel, O., Haenseler, E., Joller-Jemelka, H. I., Oechslin, E., Minder, E. I., Rickli, H. and Fehr, T. (2003) Troponin as a risk factor for mortality in critically ill patients without acute coronary syndromes. J. Am. Coll. Cardiol. **41**, 2004–2009

11 Charpentier, J., Luyt, C-E., Fulla, Y., Visonneau, C., Cariou, A., Grabar, S., Dhainaut, J-F., Mira, J-P. and Chiche, J-D. (2004) Brain natriuretic peptide: a marker of myocardial dysfunction and prognosis during severe sepsis. Crit. Care Med. **32**, 660–665

12 Jardin, F., Fourme, T., Page, B., Loubieres, Y., Vieillard-Baron, A., Beauchet, A. and Bourdarias, J-P. (1999) Persistent preload defect in severe sepsis despite fluid loading: a longitudinal echocardiographic study in patients with septic shock. Chest **116**, 1354–1359

13 Parker, M. M., Shelhamer, J. H., Bacharach, S. L., Green, M., Natanson, C., Frederick, T. M., Deamske, B. A. and Parrillo, J. E. (1984) Profound but reversible myocardial depression in patients with septic shock. Ann. Intern. Med. **100**, 483–490

14 Brealey, D., Karyampudi, S., Jacques, T. S., Novelli, M., Stidwill, R., Taylor, V., Smolenski, R. T. and Singer, M. (2004) Mitochondrial dysfunction in a long-term rodent model of sepsis and organ failure. Am. J. Physiol. Regul. Integr. Comp. Physiol. **286**, R491–R497

15 Slama, M., Susic, D., Varagic, J., Ahn, J. and Frohlich, E. D. (2002) Echocardiographic measurement of cardiac output in rats. Am. J. Physiol. Heart Circ. Physiol. **284**, H691–H697

16 Huber, W., von Heydebreck, A., Sultmann, H., Poustka, A. and Vingron, M. (2002) Variance stabilization applied to microarray data calibration and to the quantification of differential expression. Bioinformatics **18**, S96–S104

17 Azimi, G. and Vincent, J-L. (1986) Ultimate survival from septic shock. Resuscitation **14**, 245–253

18 Kumar, A., Schupp, E., Bunnell, E., Ali, A., Milcarek, B. and Parrillo, J. E. (2008) Cardiovascular response to dobutamine stress predicts outcome in severe sepsis and septic shock. Crit. Care **12**, R35

19 Tuchschmidt, J., Fried, J., Astiz, M. and Rackow, E. (1992) Elevation of cardiac output and oxygen delivery improves outcome in septic shock. Chest **102**, 216–220

20 Parrillo, J. E., Burch, C., Shelhamer, J. H., Parker, M. M., Natanson, C. and Schuette, W. (1985) A circulating mycoardial depressant substance in humans with septic shock. J. Clin. Invest. **76**, 1539–1553

21 dos Santos, C. C., Gattas, D. J., Tsoporis, J. N., Smeding, L., Kabir, G., Masoom, H., Akram, A., Plotz, F., Slutsky, A. S., Husain, M. et al. (2010) Sepsis-induced myocardial depression is associated with transcriptional changes in energy metabolism and contractile related genes: a physiological and gene expression-based approach. Crit. Care Med. **38**, 894–902

22 Hinkelbein, J., Kalenka, A., Schubert, C., Peterka, A. and Feldmann, Jr, R. E. (2010) Proteome and metabolome alterations in heart and liver indicate compromised energy production during sepsis. Protein Pept. Lett. **17**, 18–31

23 Hollenberg, S. M., Dumasius, A., Easington, C., Colilla, S. A., Neumann, A. and Parrillo, J. E. (2001) Characterization of a hyperdynamic murine model of resuscitated sepsis using echocardiography. Am. J. Respir. Crit. Care Med. **164**, 891–895

24 Jones, A. E., Craddock, P. A., Tayal, V. S. and Kline, J. A. (2005) Diagnostic accuracy of left ventricular function for identifying sepsis among emergency department patients with nontraumatic symptomatic undifferentiated hypotension. Shock **24**, 513–517

25 Poelaert, J., Declerck, C., Vogelaers, D., Colardyn, F. and Visser, C. A. (1997) Left ventricular systolic and diastolic function in septic shock. Intensive Care Med. **23**, 553–560

26 Zanotti-Cavazzoni, S. L., Guglielmi, M., Parrillo, J. E., Walker, T., Dellinger, R. P. and Hollenberg, S. M. (2009) Fluid resuscitation influences cardiovascular performance and mortality in a murine model of sepsis. Intensive Care Med. **35**, 748–754

27 Hotchkiss, R. S., Swanson, P. E., Cobb, J. P., Allyson, J., Buchman, T. G. and Karl, I. E. (1997) Apoptosis in lymphoid and parenchymal cells during sepsis: findings in normal and T- and B-cell-deficient mice. Crit. Care Med. **25**, 1298–1307

28 Solomon, M. A., Correa, R., Alexander, H. R., Koev, L. A., Corb, J. P., Kim, D. K., Roberts, W. C., Quezado, Z. M. N., Scholz, T. D., Cunnion, R. E. et al. (1994) Myocardial energy metabolism and morphology in a canine model of sepsis. Am. J. Physiol. Heart Circ. Physiol. **266**, 757–768

29 Hotchkiss, R. S., Swanson, P. E., Freeman, B. D., Tinsley, K. W., Cobb, J. P., Matuschak, G. M., Buchman, T. G. and Karl, I. E. (1999) Apoptotic cell death in patients with sepsis, shock, and multiple organ dysfunction. Crit. Care Med. **27**, 1230–1248

30 Rossi, M. A., Celes, M. R., Prado, C. M. and Saggioro, F. P. (2007) Myocardial structural changes in long-term human severe sepsis/septic shock may be responsible for cardiac dysfunction. Shock **27**, 10–18

31 Hersch, M., Gnidec, A. A., Bersten, A. D., Troster, M., Rutledge, F. S. and Sibbald, W. J. (1990) Histologic and ultrastructural changes in nonpulmonary organs during early hyperdynamic sepsis. Surgery **107**, 397–410

32 Suliman, H. B., Welty-Wolf, K. E., Carraway, M. S., Tatro, L. and Piantadosi, C. A. (2004) Lipopolysaccharide induces oxidative cardiac mitochondrial damage and biogenesis. Cardiovasc. Res. **64**, 279–288

33 Watts, J. A., Kline, J. A., Thornton, L. R., Grattan, R. M. and Brar, S. S. (2004) Metabolic dysfunction and depletion of mitochondria in hearts of septic rats. J. Mol. Cell. Cardiol. **36**, 141–150

34 Cowley, R. A., Merger, W. J., Fisher, R. S., Jones, R. T. and Trump, B. F. (1979) The subcellular pathology of shock in trauma patients: studies using immediate autopsy. Am. J. Surg. **45**, 255–269

35 Levy, R. J., Piel, D. A., Acton, P. D., Zhou, R., Ferrari, V. A., Karp, J. S. and Deutschman, C. S. (2005) Evidence of myocardial hibernation in the septic heart. Crit. Care Med. **33**, 2752–2756

36 Thomas, S. A., Fallavollita, J. A., Suzuki, G., Borgers, M. and Canty, J. M. Jr. (2002) Dissociation of regional adaptations to ischemia and global myolysis in an accelerated swine model of chronic hibernating myocardium. Circ. Res. **91**, 970–977

37 Singer, M., De Santis, V., Vitale, D. and Jeffcoate, W. (2004) Multiorgan failure is an adaptive, endocrine-mediated, metabolic response to overwhelming systemic inflammation. Lancet **364**, 545–548

38 Calvano, S. E., Xiao, W., Richards, D. R., Felciano, R. M., Baker, H. V., Cho, R. J., Chen, R. O., Brownstein, B. H., Cobb, J. P., Tschoeke, S. K. et al. (2005) A network-based analysis of systemic inflammation in humans. Nature **437**, 1032–1037

39 Zou, L., Feng, Y., Chen, Y. J., Si, R., Shen, S., Zhou, Q., Ichinose, F., Scherrer-Crosbie, M. and Chao, W. (2010) Toll-like receptor 2 plays a critical role in cardiac dysfunction during polymicrobial sepsis. Crit. Care Med. **38**, 1335–1342

40 Booz, G. W., Day, J. N. and Baker, K. M. (2002) Interplay between the cardiac renin angiotensin system and JAK-STAT signaling: role in cardiac hypertrophy, ischemia/reperfusion dysfunction, and heart failure. J. Mol. Cell. Cardiol. **34**, 1443–1453

41 Mascareno, E., El-Shafei, M., Maulik, N., Sato, M., Guo, Y., Das, D. K. and Siddiqui, M. A. (2001) JAK/STAT signaling is associated with cardiac dysfunction during ischemia and reperfusion. Circulation **104**, 325–329

42 Hui, L., Yao, Y., Wang, S., Yu, Y., Dong, N., Li, H. and Sheng, Z. (2009) Inhibition of Janus kinase 2 and signal transduction and activator of transcription 3 protect against cecal ligation and puncture-induced multiple organ damage and mortality. J. Trauma **66**, 859–865

43 Kass, D. A., Takimoto, E., Nagayama, T. and Champion, H. C. (2007) Phosphodiesterase regulation of nitric oxide signaling. Cardiovasc. Res. **75**, 303–314

44 Pathak, A., del Monte, F., Zhao, W., Schultz, J. E., Lorenz, J. N., Bodi, I., Weiser, D., Hahn, H., Carr, A. N., Syed, F. et al. (2005) Enhancement of cardiac function and suppression of heart failure progression by inhibition of protein phosphatase 1. Circ. Res. **96**, 756–766

45 Periasamy, M. and Huke, S. (2001) SERCA pump level is a critical determinant of Ca^{2+} homeostasis and cardiac contractility. J. Mol. Cell. Cardiol. **33**, 1053–1063
46 du Bell, W. H. and Rogers, T. B. (2004) Protein phosphatase 1 and an opposing protein kinase regulate steady-state L-type Ca^{2+} current in mouse cardiac myocytes. J. Physiol. **556**, 79–93
47 Stengl, M., Bartak, F., Sykora, R., Chvojka, J., Benes, J., Krouzecky, A., Novak, I., Sviglerova, J., Kuncova, J. and Matejovic, M. (2010) Reduced L-type calcium current in ventricular myocytes from pigs with hyperdynamic septic shock. Crit. Care Med. **38**, 579–587
48 Duncan, D. J., Yang, Z., Hopkins, P. M., Steele, D. S. and Harrison, S. M. (2010) TNF-α and IL-1β increase Ca^{2+} leak from the sarcoplasmic reticulum and susceptibility to arrhythmia in rat ventricular myocytes. Cell Calcium **47**, 378–386
49 Recknagel, P., Gonnert, F. A, Westermann, M., Lambeck, S., Lupp, A., Rudiger, A., Dyson, A., Carré, J. E., Kortgen, A., Krafft, C. et al. (2012) Liver dysfunction and phosphatidylinositol-3-kinase signaling in early sepsis: experimental studies in rodent models of peritonitis. PLoS Med. **9**, e1001338

Received 25 June 2012/31 August 2012; accepted 18 September 2012
Published as Immediate Publication 18 September 2012, doi: 10.1042/CS20120334

Clinical Science (2013) **124**, 391–401 (Printed in Great Britain) doi: 10.1042/CS20120334

Original Paper

SUPPLEMENTARY ONLINE DATA

Early functional and transcriptomic changes in the myocardium predict outcome in a long-term rat model of sepsis

Alain RUDIGER*, Alex DYSON*, Karen FELSMANN†, Jane E. CARRÉ*, Valerie TAYLOR*, Sian HUGHES‡, Innes CLATWORTHY§, Alessandro PROTTI*, Denis PELLERIN‖, Jana LEMM¶, Ralf A. CLAUS¶, Michael BAUER¶[1] and Mervyn SINGER*

*Bloomsbury Institute of Intensive Care Medicine, Division of Medicine, University College London, Gower Street, London WC1E 6BT, U.K.
†SIRS-Lab GmbH, Otto-Schott-Straße 15, D-07745 Jena, Germany
‡Department of Histopathology, Royal Free and University College Medical School, University College London, Rockefeller Building, University Street, London WC1E 6JJ, U.K.
§Imaging Facility, UCL Institute of Opthalmology, 11–43 Bath Street, London EC1V 9EL. U.K.
‖The Heart Hospital, UCL Hospitals NHS Foundation Trust, 16-18 Westmoreland Street, London W1G 8PH, U.K.
¶Integrated Research and Treatment Center–Center for Sepsis Control and Care, Jena University Hospital, Allee 101, D-07747 Jena, Germany

Table S1 Reproducibility of echocardiography parameters

Intra-observer variability is the variability between two analyses of the same study. Inter-observer variability is the variability between two observers analysing the same study. Inter-study variability is the variability between data acquired at two time-points within 24 h, recorded and analysed by one investigator. Variability is calculated as the difference between two observations divided by the mean of the two observations and expressed as percentage. LV EDV, LV end-diastolic volume; LV EF, LV ejection fraction; IVC inferior vena cava.

	Naïve animals ($n = 10$)			Animals with sepsis at 6 h ($n = 10$)	
Paramter	Intra-observer variability (%)	Inter-observer variability (%)	Inter-study variability (%)	Intra-observer variability (%)	Inter-observer variability (%)
HR (beats/min)	0.39 (0.14)	0.63 (0.10)	6.7 (1.4)	0.70 (0.13)	0.85 (0.19)
LV EDV (ml)	4.5 (1.2)	7.7 (1.7)	8.8 (2.3)	8.1 (1.5)	8.9 (2.0)
Stroke volume (ml)	2.1 (0.35)	3.6 (0.7)	6.1 (1.7)	7.8 (1.6)	6.4 (1.1)
Cardiac output (ml/min)	1.9 (0.35)	3.9 (0.79)	3.9 (0.78)	7.5 (1.5)	5.9 (1.1)
LV EF (%)	5.1 (1.2)	5.8 (1.2)	8.2 (1.9)	11 (2.3)	14 (2.8)
IVC diameter (mm)	5.4 (1.1)	7.6 (2.4)	13 (3.7)	6.8 (2.1)	3.5 (1.3)

[1] A member of the scientific advisory board of SIRS-Lab GmbH, Jena, Germany, where the microarray experiments were performed.

Correspondence: Professor Mervyn Singer (email m.singer@ucl.ac.uk).

Table S2 Genes significantly up-regulated or down-regulated in predicted sepsis non-survivors compared with survivors (clusters 1 and 3)

Molecule	Gene regulation	Description	Location	Type
ABCG3 (includes EG:27405)	Down	ABC (ATP-binding cassette), sub-family G (WHITE), member 3	Plasma membrane	Transporter
AFF4	Up	AF4/FMR2 family, member 4	Nucleus	Transcription regulator
ALMS1	Down	Alstrom syndrome 1	Cytoplasm	Other
APLN	Down	apelin, AGTRL1 ligand	Extracellular space	Other
APOBEC3F	Up	Apo B (apolipoprotein B) mRNA editing enzyme, catalytic polypeptide-like 3F	Unknown	Enzyme
ARHGEF9	Down	Cdc42 GEF (guanine-nucleotide-exchange factor) 9	Cytoplasm	Other
ARL5A	Up	Arf (ADP-ribosylation factor)-like 5A	Unknown	Enzyme
ATP2A3	Down	ATPase, Ca^{2+} transporting, ubiquitous	Cytoplasm	Transporter
BCL10	Up	B-cell CLL/lymphoma 10	Cytoplasm	Transcription regulator
BCR	Up	Breakpoint cluster region	Cytoplasm	Kinase
BTG2	Up	BTG family, member 2	Nucleus	Transcription regulator
C11ORF54	Down	Chromosome 11 open reading frame 54	Nucleus	Other
C14ORF172	Up	Chromosome 14 open reading frame 172	Unknown	Enzyme
C4ORF14	Up	Chromosome 4 open reading frame 14	Cytoplasm	Other
CC2D2A	Down	Coiled-coil and C2 domain containing 2A	Unknown	Other
CD55	Up	CD55 molecule, decay accelerating factor for complement (Cromer blood group)	Plasma membrane	Other
CDC42SE1	Up	CDC42 small effector 1	Plasma membrane	Other
CDK5	Down	Cyclin-dependent kinase 5	Nucleus	Kinase
CDKN1A	Up	cyclin-dependent kinase inhibitor 1A (p21, Cip1)	Nucleus	Kinase
CES1 (includes EG:1066)	Up	Carboxylesterase 1 (monocyte/macrophage serine esterase 1)	Cytoplasm	Enzyme
CH25H	Up	Cholesterol 25-hydroxylase	Cytoplasm	Enzyme
CLCN3	Up	Chloride channel 3	Plasma membrane	Ion channel
CYB5R2	Down	Cytochrome b5 reductase 2	Unknown	Enzyme
CYP2U1	Down	Cytochrome *P*-450, family 2, subfamily U, polypeptide 1	Unknown	Enzyme
DDB2	Down	Damage-specific DNA binding protein 2, 48kDa	Nucleus	Other
DDIT4L	Down	DNA-damage-inducible transcript 4-like	Unknown	Other
DEPDC7	Up	DEP domain containing 7	Unknown	Other
DTWD1	Down	DTW domain containing 1	Unknown	Other
DUSP11	Up	Dual specificity phosphatase 11 (RNA/RNP complex 1-interacting)	Nucleus	Phosphatase
EGFLAM	Down	EGF-like, fibronectin type III and laminin G domains	Unknown	Other
ENPP1	Down	Ectonucleotide pyrophosphatase/phosphodiesterase 1	Plasma membrane	Enzyme
EVL	Down	Enah/Vasp-like	Cytoplasm	Other
FAM81A	Down	Family with sequence similarity 81, member A	Unknown	Other
FHL1	Up	four and a half LIM domains 1	Cytoplasm	Other
FLJ21865	Down	Endo-β-N-acetylglucosaminidase	Unknown	Enzyme
FLNC	Up	Filamin C, gamma (actin binding protein 280)	Cytoplasm	Other
FOXK2	Up	Forkhead box K2	Nucleus	Transcription regulator
GADD45G	Up	Growth arrest and DNA-damage-inducible, gamma	Nucleus	Other
GALM	Down	Galactose mutarotase (aldose 1-epimerase)	Cytoplasm	Enzyme
GALNACT-2	Up	Chondroitin sulfate GalNAcT-2	Cytoplasm	Enzyme

Table S2 Continued

Molecule	Gene regulation	Description	Location	Type
GCGR	Down	Glucagon receptor	Plasma membrane	G-protein coupled receptor
GEM	Up	GTP-binding protein overexpressed in skeletal muscle	Plasma membrane	Enzyme
GRN	Down	Granulin	Extracellular space	Growth factor
HAS1	Up	Hyaluronan synthase 1	Plasma membrane	Enzyme
HIP1	Down	Huntingtin interacting protein 1	Cytoplasm	Other
HRSP12	Down	Heat-responsive protein 12	Cytoplasm	Other
ITPKC	Up	Inositol 1,4,5-trisphosphate 3-kinase C	Unknown	Kinase
JAG2	Down	jagged 2	Extracellular space	Growth factor
KCNK2	Down	Potassium channel, subfamily K, member 2	Plasma membrane	Ion channel
KRCC1	Up	Lysine-rich coiled-coil 1	Unknown	Other
LOC499828	Up	Similar to copine VIII isoform 1	Unknown	Other
MAGED2	Down	melanoma antigen family D, 2	Plasma membrane	Other
MAP2K6	Down	Mitogen-activated protein kinase kinase 6	Cytoplasm	Kinase
MATN2	Down	Matrilin 2	Extracellular space	Other
MDM1	Down	Mdm4, transformed 3T3 cell double minute 1, p53 binding protein (mouse)	Unknown	Other
METTL6	Up	Methyltransferase like 6	Unknown	Enzyme
MGC70857	Down	Similar to RIKEN cDNA C030006K11 gene	Unknown	Other
MLL5	Down	Myeloid/lymphoid or mixed-lineage leukemia 5 (trithorax homologue, *Drosophila*)	Nucleus	Other
MMD	Down	Monocyte to macrophage differentiation-associated	Plasma membrane	Other
MRTO4	Up	mRNA turnover 4 homologue (*S. cerevisiae*)	Cytoplasm	Other
MYC	Up	v-myc myelocytomatosis viral oncogene homologue (avian)	Nucleus	Transcription regulator
MYOT	Up	Myotilin	Cytoplasm	Other
NCF4	Up	Neutrophil cytosolic factor 4, 40 kDa	Cytoplasm	Enzyme
NR0B2	Down	Nuclear receptor subfamily 0, group B, member 2	Nucleus	Ligand-dependent nuclear receptor
NRM	Down	Nurim (nuclear envelope membrane protein)	Nucleus	Other
NSUN5	Up	NOL1/NOP2/Sun domain family, member 5	Unknown	Other
OLR1117 PREDICTED	Up	Olfactory receptor 1117 (predicted)	Plasma membrane	G-protein coupled receptor
OPN4	Up	Opsin 4 (melanopsin)	Plasma membrane	G-protein coupled receptor
OR51E2	Down	Olfactory receptor, family 51, subfamily E, member 2	Plasma membrane	G-protein coupled receptor
PDE10A	Up	Phosphodiesterase 10A	Cytoplasm	Enzyme
PIK3IP1	Down	Phosphoinositide-3-kinase interacting protein 1	Unknown	Other
PPP1CB	Up	Protein phosphatase 1, catalytic subunit, β isoform	Cytoplasm	Phosphatase
PPP1R15A (includes EG:23645)	Up	Protein phosphatase 1, regulatory (inhibitor) subunit 15A	Cytoplasm	Other
PUS7	Up	Pseudouridylate synthase 7 homologue (*S. cerevisiae*)	Unknown	Other
PVR	Up	poliovirus receptor	Plasma membrane	G-protein coupled receptor
RAB40B	Down	RAB40B, member RAS oncogene family	Plasma membrane	Enzyme
RBM13	Up	RNA binding motif protein 13	Nucleus	Other
REL	Up	v-rel reticuloendotheliosis viral oncogene homologue (avian)	Nucleus	Transcription regulator
RGD1559728 PREDICTED	Up	RGD1559728 (predicted)	Unknown	Other
RGD1559957 PREDICTED	Up	RGD1559957 (predicted)	Unknown	Other
RGD1561949 PREDICTED	Up	Similar to spermidine synthase (predicted)	Unknown	Other

Table S2 Continued

Molecule	Gene regulation	Description	Location	Type
RGD1562388 PREDICTED	Down	Similar to ORF2 consensus sequence encoding endonuclease and reverse transcriptase minus RNaseH (predicted)	Unknown	Other
RGD1564483 PREDICTED	Up	Similar to ARP2/3 complex 16 kDa subunit (p16-ARC) (predicted)	Unknown	Other
RGD1564567 PREDICTED	Up	Similar to CG14998-PC, isoform C (predicted)	Unknown	Other
RGS2	Up	Regulator of G-protein signalling 2, 24kDa	Nucleus	Other
RND1	Up	Rho family GTPase 1	Cytoplasm	Enzyme
RYR3	Up	Ryanodine receptor 3	Plasma membrane	Ion channel
SCRIB	Down	Scribbled homologue (*Drosophila*)	Cytoplasm	Other
SCRN1	Down	Secernin 1	Cytoplasm	Other
SELP	Up	Selectin P (granule membrane protein 140 kDa, antigen CD62)	Plasma membrane	Other
SH3BGRL2	Up	SH3 domain binding glutamic acid-rich protein like 2	Plasma membrane	Other
SIAH2	Up	Seven in absentia homologue 2 (*Drosophila*)	Nucleus	Transcription regulator
SLC20A1	Up	Solute carrier family 20 (phosphate transporter), member 1	Plasma membrane	Transporter
SLC37A2	Down	Solute carrier family 37 (glycerol-3-phosphate transporter), member 2	Unknown	Transporter
SLC37A4	Down	Solute carrier family 37 (glucose-6-phosphate transporter), member 4	Cytoplasm	Transporter
SNRPA1	Up	Small nuclear ribonucleoprotein polypeptide A'	Nucleus	Other
SOX4	Down	SRY (sex-determining region Y)-box 4	Nucleus	Transcription regulator
SP3	Up	Sp3 transcription factor	Nucleus	Transcription regulator
STAB1	Down	Stabilin 1	Plasma membrane	Transporter
STAG1	Up	Stromal antigen 1	Nucleus	Other
STAT3	Up	Signal transducer and activator of transcription 3 (acute-phase response factor)	Nucleus	Transcription regulator
TCF3	Down	Transcription factor 3 (E2A immunoglobulin enhancer binding factors E12/E47)	Nucleus	Transcription regulator
TGS1	Up	Trimethylguanosine synthase homologue (*S. cerevisiae*)	Nucleus	Transcription regulator
TMEM53	Down	*trans*-Membrane protein 53	Unknown	Other
TP53I11	Down	Tumour protein p53 inducible protein 11	Unknown	Other
TREM2	Down	Triggering receptor expressed on myeloid cells 2	Plasma membrane	*trans*-membrane receptor
TRH	Up	Thyrotropin-releasing hormone	Extracellular space	Other
TRIB1	Up	Tribbles homologue 1 (*Drosophila*)	Cytoplasm	Kinase
TUBB6	Up	Tubulin, β 6	Cytoplasm	Other
UAP1	Up	UDP-N-acetylglucosamine pyrophosphorylase 1	Nucleus	Enzyme
UNC5C	Down	unc-5 homologue C (*C. elegans*)	Plasma membrane	*trans*-membrane receptor
UROD	Down	Uroporphyrinogen decarboxylase	Cytoplasm	Enzyme
USPL1	Up	Ubiquitin specific peptidase like 1	Unknown	Other
VPS45	Down	Vacuolar protein sorting 45 homologue (*S. cerevisiae*)	Cytoplasm	Transporter
WDR60	Down	WD repeat domain 60	Unknown	Other
WDR67	Down	WD repeat domain 67	Unknown	Other
XIRP1	Up	Xin actin-binding repeat containing 1	Plasma membrane	Other
ZFP472	Down	Zinc finger protein 472	Unknown	Other
ZFP61	Down	Zinc finger protein 61	Unknown	Peptidase
ZMYND19	Up	Zinc finger, MYND-type containing 19	Plasma membrane	Other

Table S3 Correlation between gene array and PCR values
Correlations between gene array and real-time PCR values for ATP2A3, PRKAG2, PRKACA and PPP1CB.

Gene	Pearson's correlation coefficient (r)	Square of the correlation coefficient (R^2)	P value
ATP2A3 ($n = 16$)	0.802	0.643	<**0.001**
PRKAG2 ($n = 16$)	0.753	0.567	**0.001**
PRKACA ($n = 14$)	0.625	0.391	**0.017**
PPP1CB ($n = 16$)	0.201	0.040	0.455

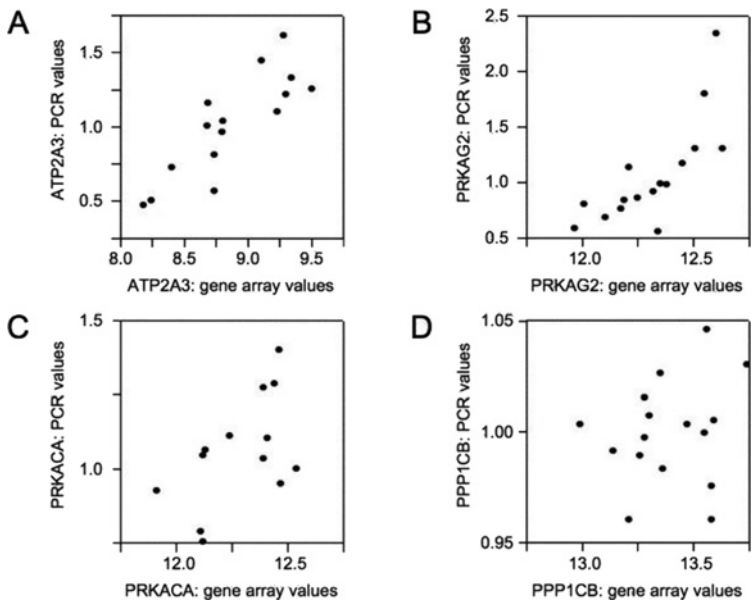

Figure S1 Correlation between gene array and real-time PCR values
(**A**) ATP2A3, (**B**) PRKAG2, (**C**) PRKACA and (**D**) PPP1CB. PCR results are given as the ratio between the gene of interest and the housekeeping gene HMBS.

Received 25 June 2012/31 August 2012; accepted 18 September 2012
Published as Immediate Publication 18 September 2012, doi: 10.1042/CS20120334